(p,n) quasifree excitations in p-shell nuclei at 186 MeV

L. Wang, X. Yang, and J. Rapaport
Ohio University, Athens, Ohio 45701

C. D. Goodman, C. C. Foster, and Y. Wang
Indiana University Cyclotron Facility, Indiana University, Bloomington, Indiana 47405

J. Piekarewicz
Florida State University, Tallahassee, Florida 32306

E. Sugarbaker, D. Marchlenski, S. de Lucia, and B. Luther
Ohio State University, Columbus, Ohio 43210

L. Rybarcyk and T. N. Taddeucci
Los Alamos National Laboratory, Los Alamos, New Mexico 87545

B. K. Park
New Mexico State University, Las Cruces, New Mexico 88003
(Received 27 June 1994)

Double differential cross sections for (p,n) quasifree scattering on p-shell nuclei, ^{6,7}Li, ^{10,11}B, and ^{12,13}C, have been measured at an incident proton energy of 186 MeV between $\theta_{\rm lab} = 0°$ and $\theta_{\rm lab} = 50°$ in steps of 5°. The normal polarization transfer coefficient, analyzing power, and induced polarization were also measured at $\theta_{\rm lab} = 0°$, 15°, and 20° using an incident proton beam of transverse polarization. Calculations by some competing quasifree models are presented and compared with the experimental results.

PACS number(s): 25.40.Ep, 27.20.+n, 24.70.+s

I. INTRODUCTION

The quasifree (QF) region represents a broad peak in the nuclear continuum which may be viewed as an elastic collision of the incident particle with a single target nucleon near the nuclear surface [1] . This process becomes the dominant feature of nucleon scattering spectra observed at momentum transfers, q, between 1 and 3 fm^{-1}, and at an energy loss ω between 50 and 150 MeV irrelevant of the probe used in the nuclear excitation. The location of the maximum of the quasifree peak is expected to occur for values of $\omega \sim q^2/2m$. The width of the broad peak is related to the Fermi motion of nucleons in nuclei.

Quasifree electron scattering studies in nuclei have been reported by several authors [2,3] discussing in particular the systematics on the location of the centroid of the QF peak, which is observed at a higher excitation energy than the value expected from scattering on a free nucleon. This has been interpreted either as (a) an average nucleon interaction energy [4] that must be supplied to knock the nucleon out of the nucleus, (b) as a measure of the effective mass of the nucleon in the nucleus [3], or (c) in terms of a momentum-dependent interactive potential [5]. The area under the quasifree peak is observed to scale with mass number A.

Relativistic effects on nucleon scattering quasielastic spin observables have been studied by Horowitz and Murdock [6] and more recently by Hillhouse and De Kock [7]. These authors point out that at incident energies below 200 MeV, relativistic calculations for D_{NN} in the QF region are most sensitive to the choice between the pseudovector or pseudoscalar form of the pion coupling and that at these energies spin-orbit distortions have no effect on this observable.

One of the major efforts in recent nucleon QF experiments has been directed to obtain empirical results for the spin-longitudinal and spin-transverse nuclear responses. It is well known that inelastic electron scattering provides only information on the spin-transverse response and thus nucleon scattering results are needed to obtain the longitudinal response. Alberico *et al.* [8] have pointed out that pionic nuclear effects should be important in the QF region. The authors argued that the particle-hole interaction in the $\sigma\tau$ channel, at high energy loss and high momentum transfer, may be sufficiently attractive to produce an enhancement and shift of the spin-longitudinal response toward lower excitation energies relative to the free Fermi gas response. On the other hand the spin-transverse response should be quenched and shifted upwards in excitation energy because of the repulsiveness of the particle-hole interaction in this channel. This hardening of the isovector spin-transverse response appears well established according to the available data and analysis by Meziani *et al.* [9] of inelastic electron scattering for ^{40,48}Ca and ^{56}Fe.

The experimental results on QF excitation with heavier probes such as the $(^3\mathrm{He},t)$ [10] and the $(d,2p)$ [11]

seem to indicate a shift of the centroid of the QF peak position relative to the location of the centroid observed in inelastic electron scattering [2] which seemed to agree with the theoretical observations of Alberico *et al.* However, recent $^{12}C(\vec{p},\vec{n})$ results at $E_p = 494$ MeV [12,13] indicate that the centroid of the QF peak position agrees well with that of the $^{12}C(e,e')$ results. Another explanation has been offered for the results with heavier probes [11].

In a recent paper Wambach [14] offers an explanation for the observed probe dependence of the quasielastic peak position.

The first measurement of the spin-longitudinal nuclear response were reported by Carey *et al.* [15,16] by carrying out a complete set of D_{ij} measurements for $(\vec{p},\vec{p}\,')$ scattering at $E_p = 500$ MeV and $q = 1.75$ fm^{-1}. The ratio of the spin-longitudinal and spin-transverse responses, which should deviate considerably from unity if a collective enhancement on the spin-longitudinal channel were present, was found to be unity, contradicting the above prediction. More recently Chen *et al.* [17] report measurements for the complete set of spin observables in the $^{12}C(\vec{p},\vec{n})$ reaction at 494 MeV and $q = 1.75$ fm^{-1}. These results, which provide the single isovector spin-isospin response without the mixed isoscalar contribution present in the $(\vec{p},\vec{p}\,')$ reaction, also report a ratio of the spin responses close to unity. Several authors have recently addressed this problem [18–23].

In the present paper we present QF differential cross section results obtained in p-shell nuclei using the (p,n) charge-exchange reaction with 186 MeV incident protons. We also report values for the spin observables A_Y, P, and D_{NN} obtained at $\theta_{\rm lab} = 15°$ and 20°.

II. EXPERIMENTAL SETUP AND DATA ANALYSIS

The experiment was performed at the Indiana University Cyclotron Facility (IUCF) using 186 MeV protons. Details about the experimental setup and data analysis are given in Refs. [24,25]. Only a brief account is presented here.

Differential cross sections measurements were done with an unpolarized proton beam and two detector stations at the IUCF swinger neutron time-of-flight (TOF) facility. These detector stations were located on the 0° beam line 101 m away from the target and at the 24° beam line 62 m from the target, respectively. With this setup, data were taken in the angular range between $\theta_{\rm lab} = 0°$ and 50°, in steps of 5°. Typical intrinsic time resolution of the neutron detectors was better than 500 ps. However, the count rate was optimized with targets of about 100 mg/cm^2 and overall neutron energy resolutions of about 1 MeV in the 0° beam line detector station and about 1.3 MeV in the 24° beam line detector station were observed.

The polarization observables were measured with the IUCF polarimeter [26] using a transverse polarized proton beam. Three data sets for the normal polarization transfer coefficient (D_{NN}), the analyzing power (A_Y), and the induced polarization (P) were measured at $\theta_{\rm lab} = 0°$, 15°, and 20°.

The following targets were used in this study: ^{6,7}Li, ^{10,11}B, and ^{12,13}C. All these targets had an enrichment better than 96% and were about 100 mg/cm^2 thick.

III. RESULTS

The obtained (p,n) double differential cross section data of QF scattering on p-shell nuclei, with momentum transfer up to 2.5 fm^{-1}, provide a rich collection of data for a systematic study of shapes and centroids of the QF peak at an incident energy of 186 MeV. Similarly the results for spin observables up to 50 MeV excitation energy at $\theta_{\rm lab}$=15° and 20° provide a good test for relativistic calculations.

A. Parametrization of empirical QF peak

In Fig. 1 we show $^{12}C(p,n)$ spectra for angles between 15° and 49° in steps of 5° where the locations of the centroids of QF peaks have been indicated with a solid line. At low excitation energy the QF region overlaps with giant resonances and some low-lying discrete-state transitions. At higher excitation energy, the QF spectra is limited by the neutron TOF range. For a quantitative analysis of the QF spectra we have used a semiphenomenological fitting procedure. This method was introduced by Erell *et al.* [27] and also used by Raywood *et al.* [28]. In this procedure, the QF peak is assumed to have a Lorentzian shape. To fit the complete spectra we assumed Gaussian peaks for transitions to low-lying states and giant resonances. The QF peak shape is given in terms of a double differential cross section as a function of excitation energy E, as follows:

$$\frac{d^2\sigma}{dEd\Omega} = \begin{cases} N\dfrac{1-\exp[-(E-E_0)/T_p]}{1+[(E-E_{\rm QF})/W_{\rm QF}]^2}, & E \geq E_0, \\ 0, & E \leq E_0, \end{cases} \tag{3.1}$$

where N is a q-dependent normalization factor, E_0 is the maximum cutoff energy, T_p is a cutoff energy scale parameter reflecting how far the Pauli blocking extends into the QF region, and the Lorentzian function is centered at $E_{\rm QF}$. The measured spectra have asymmetric peak shapes; thus, an asymmetry parameter $D_{\rm QF}$ has been assigned to the QF peak width $W_{\rm QF}$ such that

$$W_{\rm QF} = \begin{cases} W_L - D_{\rm QF} & \text{if } E < E_{\rm QF}, \\ W_L + D_{\rm QF} & \text{if } E \geq E_{\rm QF}. \end{cases} \tag{3.2}$$

The QF peak is completely defined by the six parameters, N, E_0, T_p, $E_{\rm QF}$, W_L, and $D_{\rm QF}$. The cutoff energy E_0 is the separation energy of the least-bound proton in the residual nucleus, and thus it is a fixed number for a given target nucleus, e.g., for $^{12}C(p,n)^{12}N$, $E_0 = 1.95$ MeV. The value of $2W_L$ represents the full width at half maximum (FWHM) of the Lorentzian peak, which in the Fermi gas model [29] is directly related to the Fermi momentum k_F:

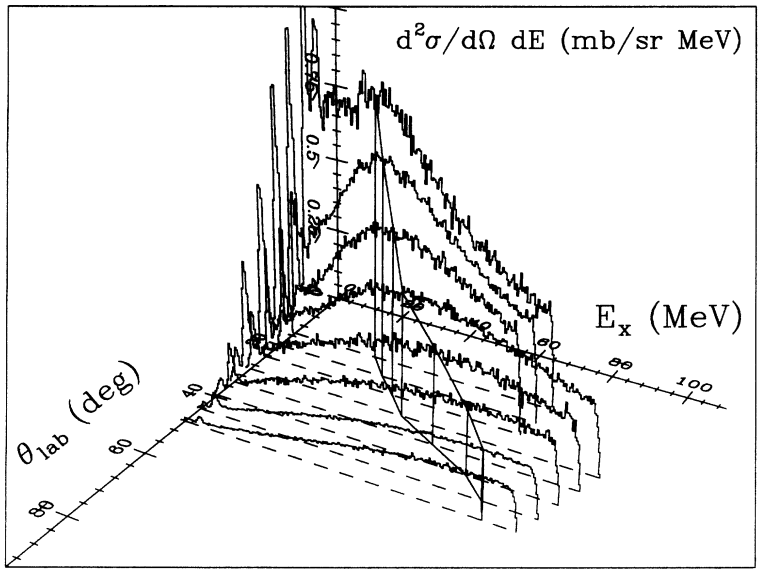

FIG. 1. Spectra obtained for the $^{12}C(p,n)^{12}N$ reaction at θ_{lab} = 15°–50° in 5° steps, at E_p=186 MeV. The solid line represents the location of the QF peak.

$$W = \frac{\sqrt{2}k_F q}{M}. \tag{3.3}$$

For scattering angles in the range $15° \leq \theta_{lab} \leq 50°$, the QF peak fitting process is straightforward because the QF peaks at these angles are well developed, and the fitting converges when all five parameters are varied. However, at angles below $\theta_{lab} < 15°$ the QF contributions are small and are mixed with contributions from excitation of giant resonances. In order to have a meaningful fitting that converges, the parameters E_{QF}, W_L, and D_{QF} were extrapolated from the values obtained at angles between $15° \leq \theta_{lab} \leq 50°$. Values for the peak position parameter E_{QF} were extrapolated to small angles by assuming a quadratic relation between the energy loss ω and momentum transfer q at the QF peak positions. The peak-fitting asymmetry parameter D_{QF} showed small variations. We choose the 15° value in the fitting procedure for angles between $0° \leq \theta_{lab} \leq 10°$. To obtain the small-angle W_L values, the following linear q^2 relation suggested by Erell *et al.* [27] was used:

$$W_L = W_{L_0}\left[1 + \alpha\left(\frac{q}{k_F}\right)^2\right]. \tag{3.4}$$

The parameter T_p, indicative of how far the Pauli blocking extends into the QF region, is a function of momentum transfer q. In the present analysis better chi squares were obtained by assuming T_p to be a function of q^2.

After the QF extraction process, a "pure" QF spectrum is obtained at each scattering angle and for each target nucleus. These empirical double differential spectra can thus be compared with calculations based on the QF scattering models. In Fig. 2 we show the $^{12}C(p,n)^{12}N$

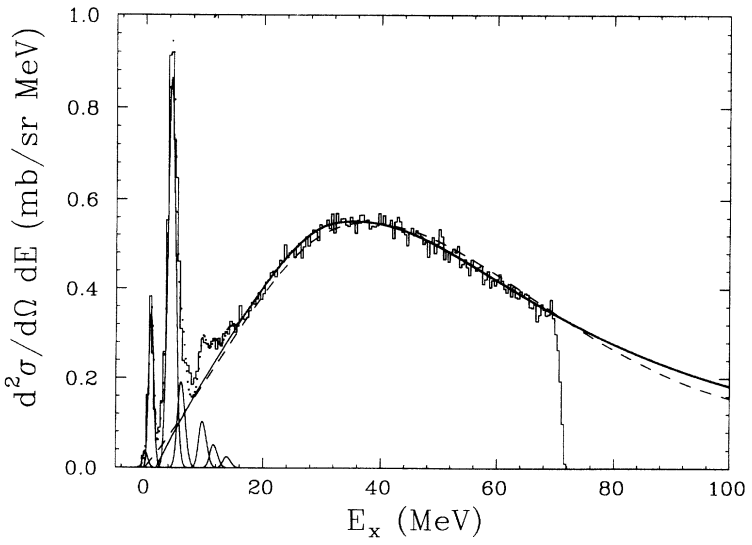

FIG. 2. The $^{12}C(p,n)^{12}N$ spectrum at θ_{lab}=25° and E_p=186 MeV. The data are plotted as a solid histogram. The individual Gaussian and QF peaks (solid lines) are easily distinguishable. Dotted curves represent the sum of the fitted curves. The dashed curve represents a slab model calculation.

spectrum obtained at $\theta_{\rm lab} = 25°$ in which the solid line represents the QF empirical parametrization and low-lying transitions are assumed to have Gaussian shapes. The dashed curve represents slab model results for the QF (see Sec. V B).

IV. QUASIFREE SCATTERING MODELS

Several theoretical models have been developed aimed at analyses of QF observables. Some of them assume infinite nuclear matter and are based on, or extended from, the simple Fermi gas model (FGM). Among these we cite the relativistic plane-wave impulse approximation (RPWIA) by Horowitz *et al.* [30,31], the nonrelativistic, interactive Fermi gas model (IFGM) by Brieva and Love [32], and the slab model by Bertsch and coworkers [33,34]. A different approach has been taken by Ichimura *et al.* [35] to develop finite nuclei theoretical calculations within a distorted wave impulse approximation (DWIA) formalism using random phase approximation (RPA) correlations in the continuum.

In the Fermi gas model, the nucleus in the ground state is treated as a Fermi sea with all states below k_F occupied. In a QF process, the struck nucleon has to be removed from the Fermi sea, and the recoiled ejectile must be left also above the Fermi sea. In this model Pauli blocking occurs when $q < 2k_F$. For a given momentum transfer q, the percentage of scattering that survives Pauli blocking can be obtained from the equation [33]

$$P(q) = \begin{cases} \frac{3}{4}\frac{q}{k_F}\left[1 - \frac{1}{12}\left(\frac{q}{k_F}\right)^2\right] & \text{if } q \le 2k_F\,, \\ 1 & \text{if } q \ge 2k_F\,. \end{cases} \tag{4.1}$$

The DWIA expression for the QF scattering double differential cross section may be factorized into three parts: (1) the normalization factor $A_{\rm eff}$; (2) the interaction part, i.e., the free nucleon-nucleon (NN) cross section $\frac{d\sigma_{NN}}{d\Omega}$; and (3) the nuclear response $S(q,\omega)$. Thus,

$$\frac{d^2\sigma(q,\omega)}{d\Omega dE} = A_{\rm eff}\sum_\alpha \left[\frac{d\sigma_{NN}}{d\Omega}\right]_\alpha S_\alpha(q,\omega)\,, \tag{4.2}$$

where the summation has been made on different spin-isospin couplings denoted by the symbol α. The factor $A_{\rm eff}$ can be interpreted as the effective number of nucleons participating in the QF scattering. Because of absorption of the incident particle, not all nucleons in the target participate in the QF scattering. The value of $A_{\rm eff}$ may be estimated using a DWIA calculation or as is most commonly done by using an eikonal approximation based on the Glauber theory [36].

The simple FGM reproduces the major features of QF scattering: (1) centroid QF peak position, (2) QF peak width attributed to the Fermi motion of target nucleons, and (3) Pauli blocking explicitly incorporated. In the interactive Fermi gas models [32], residual nucleon interactions are introduced via an RPA formalism. Details about the RPA and the response theory for the IFGM can be found in Refs. [29,37].

A relativistic approach to QF scattering has been developed by Horowitz *et al.* [30,31] and more recently by Hillhouse and De Kock [7] assuming a Fermi gas model for the target. The RPWIA calculations are usually done with or without RPA, respectively. The relativistic approach is the spirit of this model. First, it incorporates the relativistic effect of the nuclear medium by solving the Dirac equation in a mean-field potential. This effect is equivalent to replacing the nucleon mass M with an effective reduced mass M^*. Typical values of M^* for nucleons are $(0.8\text{–}0.9)M$ [31]. It is important to note that in this model a pseudoscalar or a pseudovector form for the πN coupling may be used [31], although as suggested by the soft pion scattering, the pseudovector interaction is preferred. As indicated by Hillhouse and De Kock [7] RPWIA calculated D_{NN} values are quite sensitive to the choice of the interaction.

Because of its single-step knock-out nature, QF scattering has a surface-peaking nuclear response. To properly simulate this surface effect, Bertsch and Scholten [33] developed the slab model. In this model, a semi-infinite slab is used to describe the absorption of the incoming flux. Mathematically, the surface of the slab is taken to be at z=0, and for $z < 0$ a Woods-Saxon potential is assumed. Wave functions solved in the slab region are plane waves in the x-y dimensions but distorted along the z direction. The distortion factor $A_{\rm eff}$, which is equivalent to the effective number of nucleons participating in the scattering, is calculated in an eikonal approximation using target densities obtained from electron scattering [38]. Generally, however, $A_{\rm eff}$ cannot be predicted correctly in comparison with experimental results and it is left as a normalization parameter.

V. COMPARISON OF EMPIRICAL RESULTS WITH MODELS

In the following sections data obtained from differential cross section values and polarization observables are compared with the models briefly described above.

A. Integrated QF cross section and comparison with the FGM

The semiphenomenological Lorentzian function used to describe the double differential QF cross section gives a consistent treatment of all the spectra for all targets and angles. This empirical QF spectrum was integrated at each angle to produce an angular distribution of the QF scattering on each target nucleus. Such an angular QF distribution illustrates the Pauli blocking effect which may be explicitly calculated in the FGM [see Eq. (4.1)]. Although the data were taken at given $\theta_{\rm lab}$ values, the variation in the value of the momentum transfer from its value q_m at the centroid peak position of the QF is less than 10%. The data will be labeled either with its $\theta_{\rm lab}$ value or its q_m value, interchangeably.

TABLE I. Values of the QF FWHM (W), the effective number of neutrons (N_{eff}), and the corresponding Fermi momentum (k_F) at different scattering angles for $^{12}C(p,n)$ reaction.

θ_{lab}	q (fm^{-1})	W (MeV)	k_F (fm^{-1})	N_{eff}
15.0°	0.86	61.6	1.22	
20.0°	1.11	61.8	0.95	
24.5°	1.33	73.2	0.94	
29.4°	1.56	98.3	1.08	1.7
34.4°	1.78	125.5	1.20	2.0
39.4°	2.00	156.7	1.34	2.3
44.4°	2.19	149.1	1.16	1.8
48.9°	2.35	141.2	1.03	1.6
$\bar{k}_F = 1.11 \pm 0.14$ fm^{-1};			$\overline{N}_{\text{eff}} = 1.9 \pm 0.2$	

To calculate the probability factor $P(q)$, i.e., the percentage of QF scattering, at a given momentum transfer that survives the Pauli blocking as defined by Eq. (4.1), the Fermi momentum k_F must be determined. This is done by using Eq. (3.3) with W substituted by $2W_L$ determined in the empirical fitting described earlier. An average Fermi momentum $\bar{k}_F$ is obtained from the k_F values obtained at $15° \leq \theta_{\text{lab}} \leq 50°$. In Table I we present the values for the QF peak widths W, k_F values at different angles, and the average value $\bar{k}_F$ for the $^{12}C(p,n)$ QF scattering. Similar values are available for the other nuclei [25].

TABLE II. Values for $\bar{k}_F$ and $\overline{N}_{\text{eff}}$ obtained in the analysis of (p,n) QF scattering at 186 MeV on the indicated target nuclei.

Nucleus	$\bar{k}_F$ (fm^{-1})	$\overline{N}_{\text{eff}}$
^{13}C	1.06 ± 0.16	2.4 ± 0.3
^{12}C	1.11 ± 0.14	1.9 ± 0.2
^{11}B	1.05 ± 0.15	1.9 ± 0.2
^{10}B	0.93 ± 0.10	1.5 ± 0.2
^{7}Li	0.84 ± 0.08	1.9 ± 0.1
^{6}Li	0.66 ± 0.06	1.2 ± 0.1

For scattering angles $\theta_{\text{lab}} \geq 29.4°$ (or $q > 1.5$ fm^{-1}) where Pauli blocking effects become negligible, the integrated QF cross section can be scaled to the free NN value to obtain an empirical value for A_{eff}. We quote, as usually done, the effective number of neutrons, N_{eff}, given by $N_{\text{eff}} = \left(\frac{N}{A}\right) A_{\text{eff}}$. For ^{12}C, for instance, a set of N_{eff} values was obtained for $29.4° \leq \theta_{\text{lab}} \leq 48.9°$. These values and their average N_{eff} are shown in Table I. In a recent report Sakai [39] analyzed cross sections and analyzing powers for quasifree $(\vec{p},\vec{n})$ scattering at 300 and 400 MeV in many nuclei. Using a Fermi gas model he gave the following relation for the effective number of neutrons: $N_{\text{eff}} = 0.85N^{0.5}$ where N is the number of neutrons in the target nucleus. The present results show good agreement with the above relation. Listed in Table II are the values of Fermi momentum $\bar{k}_F$ and effective

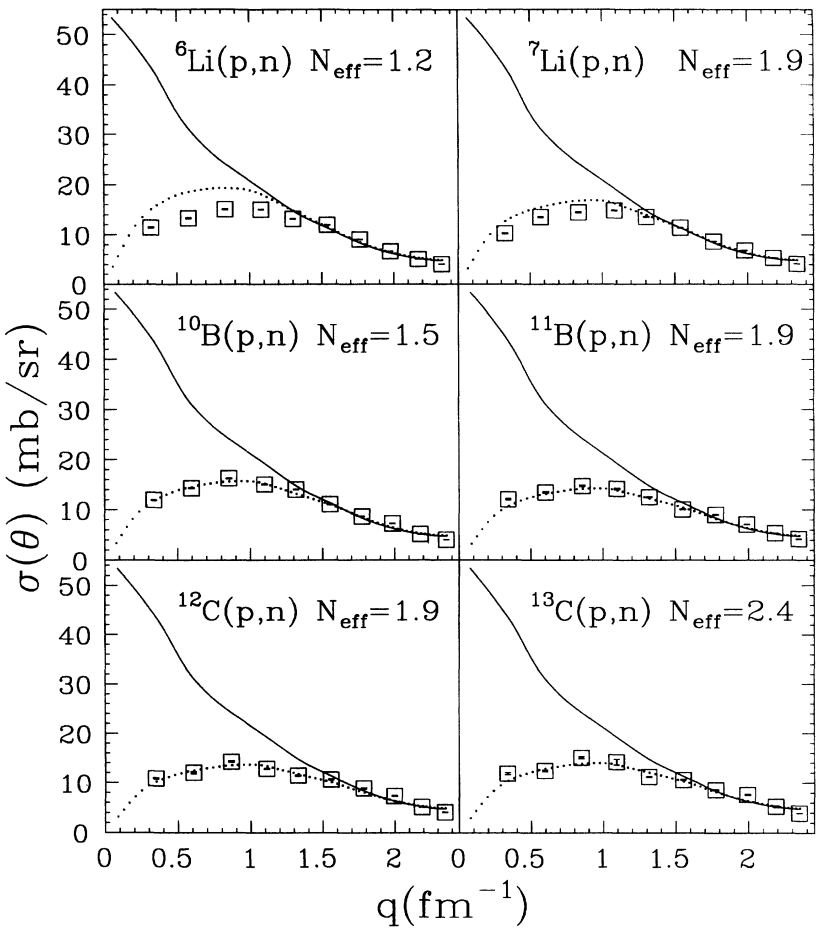

FIG. 3. Angular distribution (octagons) for integrated QF cross sections on ^{6,7}Li, ^{10,11}B, and ^{12,13}C, compared with the free NN cross section (solid line), and the free NN cross section multiplied by the Pauli blocking function $P(q)$ of Eq. (4.1) (dotted line).

number of neutrons, $\overline{N}_{\rm eff}$, obtained in the present study.

The empirical angular distributions of integrated QF cross sections for ^{6,7}Li, ^{10,11}B, and ^{12,13}C, are shown in Fig. 3, scaled by the corresponding $N_{\rm eff}$ values. Also shown in Fig. 3 are the free NN cross section from an Arndt phase shift of 1992 [45], and the same multiplied by the Pauli blocking function $P(q)$ predicted by the FGM. Good agreement is obtained between the empirical QF distribution and the FGM prediction. In the top portion of Fig. 3 the results obtained for ^{6,7}Li show a departure from the FGM predictions. This may indicate that for nuclei with mass number less than 7 the FGM statistics may no longer apply.

B. QF results compared with the slab model

1. Quasifree peak shapes

The slab model is more sophisticated than the FGM by simulating the surface response nature of the QF scattering with an explicit slab geometry. It is also more realistic in treating the nuclear response by incorporating RPA correlations in nuclear matter. In addition the slab model calculation also takes into account the Fermi motion of the struck nucleon in evaluating the two-body NN amplitudes by using "optimal amplitudes" in the "optimal frame" [40]. The shapes of the QF peak predicted by this model are in good agreement with the data (see Fig. 2) and much better than any of the other models. The ^{12}C(p,n) spectra at E_p = 186 MeV together with the empirically extracted QF peaks and the slab model calculations are shown in Fig. 4. The slab model does not predict the QF absolute cross sections. Arbitrary normalization factors are applied to the slab model calculations in order to compare the peak shapes. These normalization factors increase from 1.3 at $\theta_{\rm lab}$ = 15° to 2.1 at $\theta_{\rm lab}$ = 50° probably reflecting two-step and higher contributions not included in these calculations. It has been suggested that these contributions increase with momentum transfer [40].

For angles in the interval 15° $\leq \theta_{\rm lab} \leq$ 39°, the calculated QF peak shapes agree generally well with the empirical shapes. However, in the slab model calculation at the two largest angles, a second peak appears at a larger excitation energy which is beyond the range of excitation shown in Fig. 4. This is probably due to the breakdown of the "optimal frame" effect at large excitation energy region that is outside the range of the Fermi gas response, as discussed in Ref. [40].

The comparison between the slab model calculations and the ^{12}C data shown in Fig. 4 is a typical illustration of how the QF peak shapes are predicted by the model. Similar qualitative comparisons are expected for other light nuclei though calculations were not implemented due to the lack of ground state nuclear densities in terms of Fermi functions for these light nuclei.

2. Energies of centroids of quasifree peaks

The locations of centroids of the QF peaks were obtained using several methods varying from a simple evaluation of the peak maximum to the fitting procedures described in Sec. III A. The obtained results were in agreement within a few hundred keV. At larger angles where only part of the QF peak was measured, the use of the semiphenomenological QF function [Eq. (3.1)] and the required constrains on the W_L, T_p, and $D_{\rm QF}$ parameters allow a very good evaluation of the QF peak centroid. We estimate the uncertainties to be larger than those in the forward angles, but no more than 2 MeV (FWHM). These estimated error bars are smaller than the data symbols shown in Fig. 5.

The results are shown in Fig. 5 displayed as a function of momentum transfer q. At lower q values, the target dependences of the centroid QF peak positions are more conspicuous. The centroid values are all shifted to higher

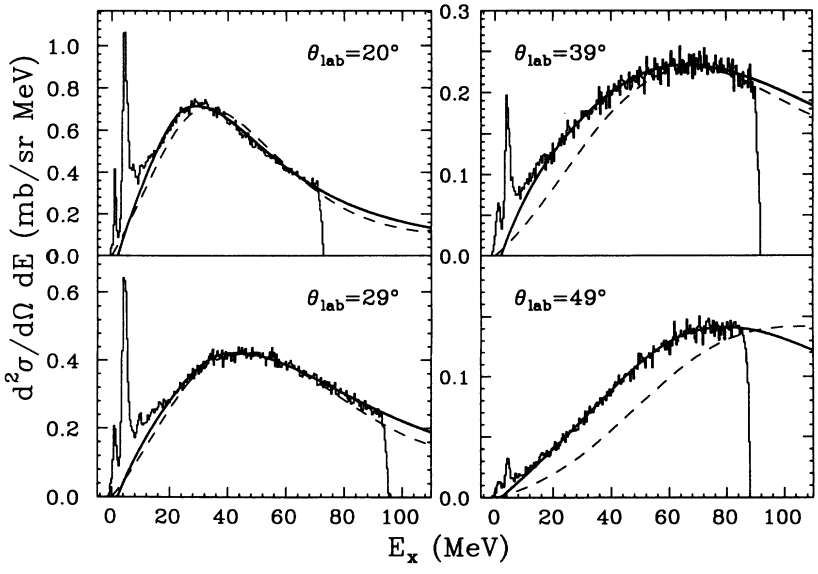

FIG. 4. The ^{12}C(p,n) spectra at $\theta_{\rm lab}$=20°, 29°, 39°, and 49°, at E_p = 186 MeV. The data are plotted as solid histograms. The dark solid line is the empirically fitted QF peak. The dashed line is the slab model calculation normalized to the empirical peak maximum.

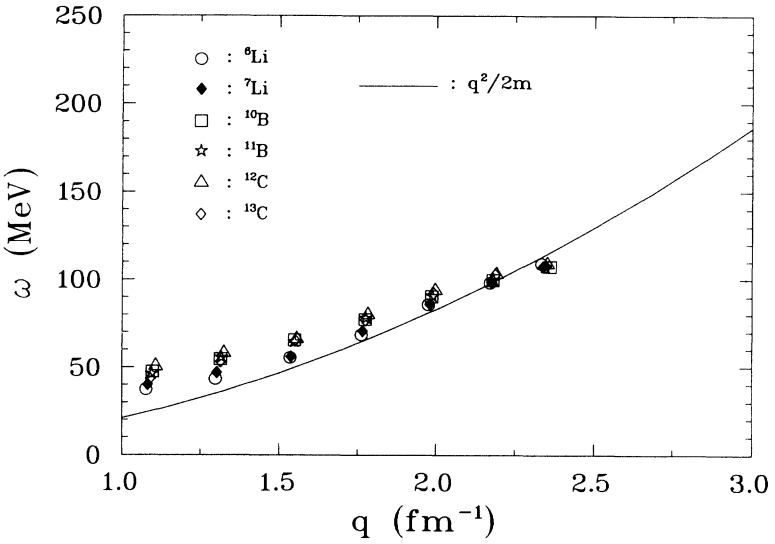

FIG. 5. Centroid QF peak positions for (p,n) reactions at $E_p = 186$ MeV, plotted as energy loss ω, vs momentum transfer q. The free NN QF peak position curve is shown as a solid line.

excitation energies with respect to the value expected for a free nucleon. However, for increasing q values, the difference between the observed centroids and that for the free nucleon-nucleon (NN) value gets smaller. Eventually, we observe that at $q \approx 2.2$ fm^{-1} the present results for the QF peak centroids cross over the free NN line. Such an interesting feature has not been observed in (p,n) reactions at higher incident energies, i.e., 495 MeV [12,13] and 795 MeV [13], or in the recent data at 300 and 400 MeV reported by Sakai [39]. In Fig. 6, adapted from Ref. [12], we show results for the centroid QF peak position for ^{12}C observed in reactions with different probes. The only reaction showing the centroid QF peak position line crossing over the free NN line in Fig. 6 is the (^{3}He,t) reaction (crossing over at $q \approx 1.9$ fm^{-1}). Gaarde [12] suggested that distortion effects in the (^{3}He,t) reaction, which are quite different from those in (p,n) reaction, could be responsible for this shift. However, in the (p,n) reaction at 186 MeV, distortions only attenuate the calculated PWIA cross section, without major effects on the QF peak shape and centroid. We believe that the "crossing-over" peak shift observed in the present (p,n) data is due to some other effects. Although we do not know the exact reasons, several possibilities are suggested. First we note that the energy dependence of the total nucleon-nucleus cross section shows a shallow minimum at about 200 MeV. This indicates that the nucleus is more transparent to the incident proton at these energies and thus it may probe deeper in the nucleus. It is known that the effect of strong pion fields is expected to be larger in denser nuclear matter [41]. Second we indicate that at an incident energy of 186 MeV the outgoing neutrons for a momentum transfer $q \sim 2$ fm^{-1} have energies less than 100 MeV. Neutrons with these energies are more attenuated in nuclear matter because of the sharp increase in the total nucleon-nucleus cross section with decreasing energy. We are theoretically studying these possibilities and at the same time we are planning to

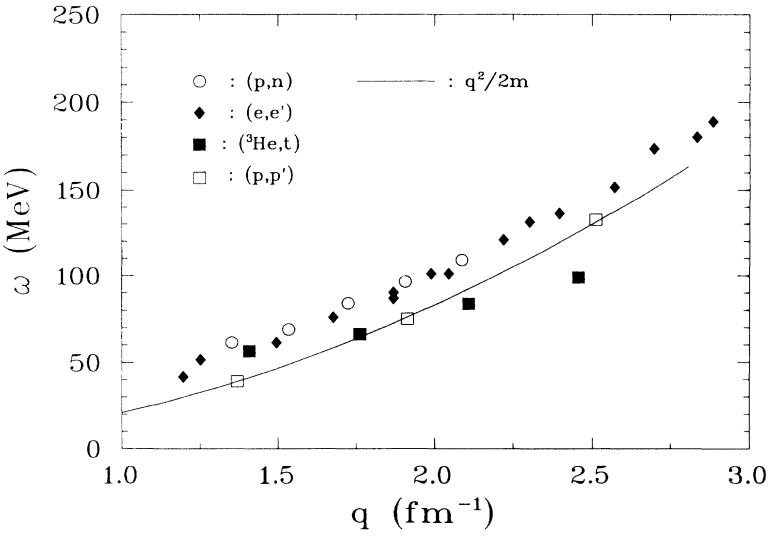

FIG. 6. The centroid QF peak position for ^{12}C as observed with different probes, plotted as energy loss ω versus momentum transfer q. Adapted from Ref. [12].

measure at $E_p = 200$ MeV the complete set of polarization transfer observables to obtain the spin-longitudinal and spin-transverse nuclear responses as done in Ref. [17].

Recently Bland [42] has carried out QF calculations for exclusive $^{12}C(p,2p)$ and $^{12}C(p,np)$ and inclusive $^{12}C(p,p')$ and $^{12}C(p,n)$ reactions, all at an incident proton energy of 200 MeV, using the code THREEDEE of Chant and Roos [43]. These calculations do a credible job of reproducing all observables and in particular the centroids QF peak location of the inclusive data, which for the (p,n) reaction were calculated at q values of 1.3 and 1.6 fm^{-1}.

C. Polarization observables and relativistic effects in the RPWIA

As discussed previously the relativistic RPWIA calculations are based on the FGM. Thus, the predicted RPWIA QF peak shapes follow basically the FGM nuclear response, which is not in good agreement with the observed QF peak shapes. The relativistic effects are incorporated in two aspects: (1) A reduced nucleon mass M^* is used in the plane-wave Dirac spinor due to mean-field effects; (2) the free NN amplitude (the "impulse" part) is parametrized in a Lorentz-invariant form in terms of relativistic interactions. These effects are especially sensitive to polarization observables [7]. Hillhouse and Kock [7] have explicitly demonstrated that D_{NN} values are by far the most sensitive observable to the two relativistic forms of the pion coupling. The present D_{NN} results are used to discriminate between the pseudoscalar and pseudovector interactions.

Although results are available for all studied light nuclei [25], we present results just for the $^{10}B(\vec{p},\vec{n})$ reaction. It provided measurements of the polarization observables with the best statistics. Also, because of the mechanism of QF scattering, the results are not expected to be strongly target dependent.

In Fig. 7 we present results on A_Y (top row), P (middle row), and D_{NN} (bottom row) for the $^{10}B(\vec{p},\vec{n})$ at $\theta_{lab} = 15°$ and 20°. Three sets of RPWIA calculations are compared with the experimental data. The solid line is the RPWIA calculation with reduced mass and pseudovector interaction, while the dotted line is a similar calculation with pseudoscalar interaction. For the incoming channel, the effective proton mass $M_1^* = 0.85M$ is used; for the outgoing channel, the effective neutron mass $M_2^* = 0.84M$ is used, where M is the free nucleon mass. The dashed line represents the RPWIA calculation with the free nucleon mass M, which is independent of the interaction [31]. The corresponding free NN values are also plotted as diagonal crosses. In agreement with the calculations for $(\vec{p},\vec{n})$ reactions at 500 MeV and 800 MeV in Ref. [31], there is almost no difference among the three RPWIA calculations for the analyzing power

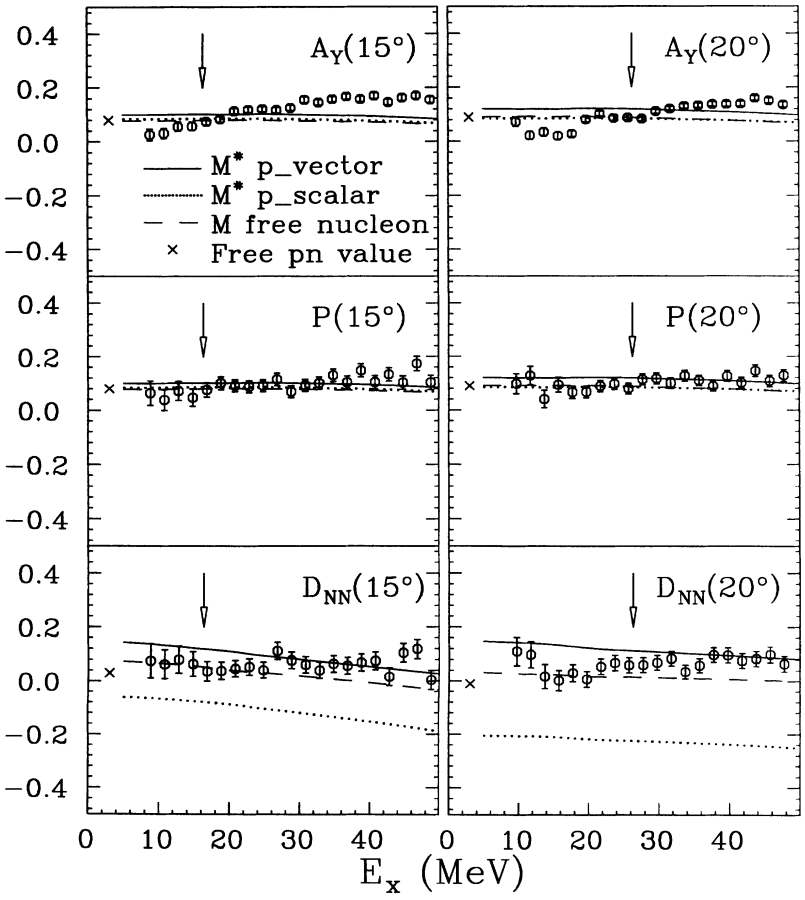

FIG. 7. Values for A_Y, P, and D_{NN} obtained in the $^{10}B(\vec{p},\vec{n})$ reaction at 186 MeV, compared with RPWIA calculations. The vertical arrow indicates the centroid of the QF peak.

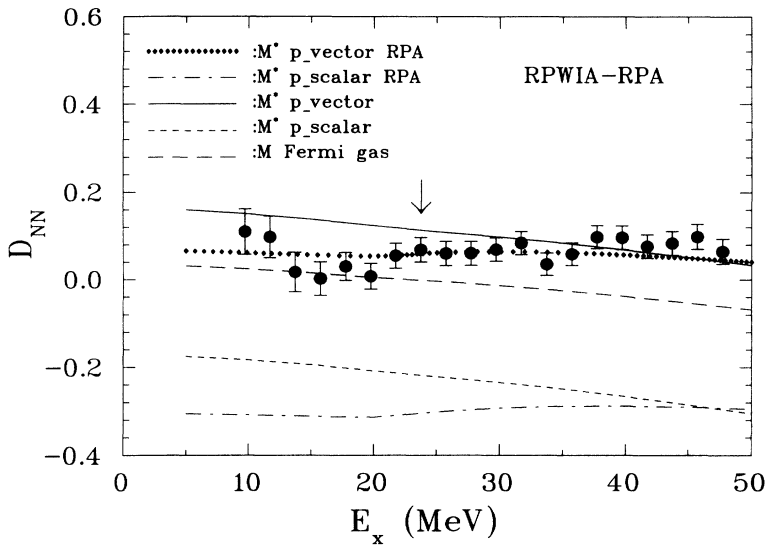

FIG. 8. Values for D_{NN} obtained in the ^{10}B$(\vec{p},\vec{n})$ reaction at E_p = 186 MeV and $\theta_{\rm lab}$ = 20° (see Fig. 7) compared with RPWIA-RPA calculations. The vertical arrow indicates the centroid of the QF peak.

A_Y, although the M^* pseudovector calculation seemed to show a closer agreement with the experimental data. As suggested in Ref. [31], this is due to the much lower sensitivity of the analyzing power to the relativistic effects in the isovector $(\vec{p},\vec{n})$ reaction than in the isoscalar-dominant $(\vec{p},\vec{p}\,')$ reaction. At both 15° and 20°, the experimental A_Y data show more a trend of enhancement in the QF region ($E_x > 30$ MeV) than is accounted for by the calculations. This is in contrast to the $(\vec{p},\vec{p}\,')$ results at energies of 300 – 800 MeV [31] where a large decrease in the analyzing power was found in comparison with the free NN values and explained by the reduced-mass effect.

Large differences are found among the calculations for the normal polarization transfer coefficient D_{NN}. Compared to the free NN values and to the calculation with free nucleon mass M, the M^* pseudovector calculation predicts higher D_{NN} values at both angles. On the contrary, the M^* pseudoscalar calculation predicts much lower D_{NN} values. The observed data show strong evidence that the pseudovector interaction is the preferred coupling for $(\vec{p},\vec{n})$ interaction at 186 MeV because it agrees well with the data. The D_{NN} data at 15° are close to the free NN values, while at 20° the data in the QF region ($E_x > 30$ MeV) are higher than the free NN values. In the lower excitation energy region ($E_x < 30$ MeV), interference between QF and the giant resonances makes the polarization observables change more drastically than in the "pure" QF region, as seen in the values for $A_Y(15°)$, $A_Y(20°)$, and $D_{NN}(20°)$.

The obtained P data are similar to the A_Y data. The RPWIA code provides no independent calculation for P, which is expected to be the same as A_Y for free NN scattering (also for QF scattering) if interactions between target nucleons are ignored. Thus the P data are compared with the RPWIA calculated A_Y curves in Fig. 7. A reasonable agreement is observed.

We have also calculated RPWIA spin observables including RPA correlations. In this approach the projectile was assumed to interact with the medium via the isovector component of the NN t matrix, parametrized

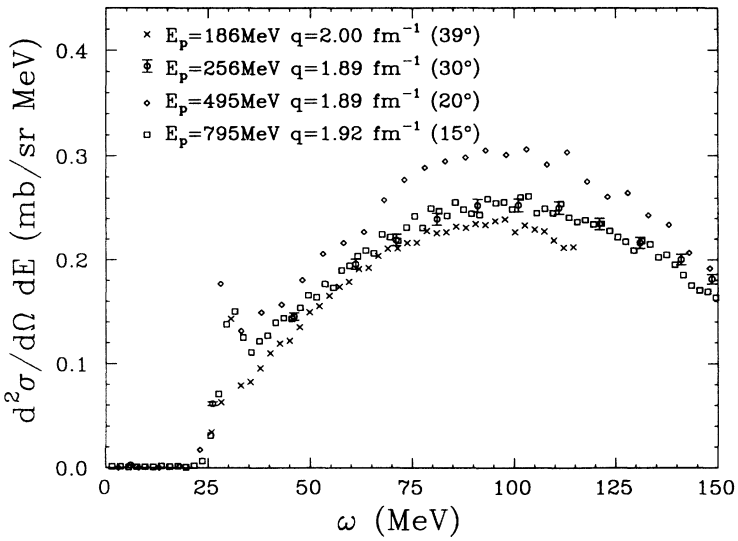

FIG. 9. Spectra for the ^{12}C(p,n) quasifree scattering at $q \approx 2$ fm^{-1} and proton energies of 186, 256, 495, and 795 MeV.

from on-shell data in a Lorentz invariant way. Nuclear-structure effects were incorporated by calculating the nuclear-matter response using a relativistic RPA to the Walecka model. For the residual interaction we have used a model based on $\pi + \rho$ exchange. Moreover, a phenomenological Landau-Migdal parameter g' was introduced to simulate the effect of repulsive short-range correlations. Isoscalar effects from a reduced nucleon mass in the medium lead to important dynamical changes in the residual interaction and, in particular, suppress the pionic enhancement predicted by nonrelativistic calculations. Further details about the calculation can be found in Ref. [18]. Similar results for pseudoscalar and pseudovector calculations are obtained as the previous RPWIA results shown in Fig. 7. The only difference is that the RPA calculation predicts better D_{NN} values in the QF region. In Fig. 8, we present the comparison of the experimental D_{NN} values at $\theta_{\rm lab} = 20°$ and the theoretical RPWIA-RPA results.

D. (p,n) quasifree scattering as a function of incident energy

It is useful to study results of nucleon QF scattering on the same target at a fixed momentum transfer q, as a function of bombarding energy. We have obtained published data for the ^{12}C(p,n) reaction at $q \sim 2$ fm^{-1} at several energies. These results are presented in Fig. 9. The data obtained in the present experiment at $\theta_{\rm lab} = 39°$ are compared with spectra obtained at $E_p = 256$ MeV, 30° [44], $E_p = 495$ MeV, 20° [13], and $E_p = 795$ MeV, 15° [13]. The momentum transfers at the centroid of the QF peaks for the four spectra are 2.00, 1.89, 1.89, and 1.92 fm^{-1}, in increasing order of bombarding energy, respectively. The empirical QF peak fitting procedure introduced earlier was applied to all the spectra. The data at 795 MeV extend substantially into the Δ-resonance region. The QF fits were confined to the energy loss range $36 \leq \omega \leq 150$ MeV to suppress the Δ contribution at high ω as well as the low-lying contributions from discrete states and collective resonances. The analyses discussed earlier were made to obtain the Fermi momentum k_F, and the integrated quasifree cross section $\left(\frac{d\sigma}{d\Omega}\right)^{\rm QF}_{\rm intg}$ values which are listed in Table III. Also listed in Table III are the centroid QF peak locations $\omega^{\rm QF}_{\rm peak}$, the value of $\left(\frac{d^2\sigma}{d\Omega dE}\right)^{\rm QF}_{\rm peak}$, and the corresponding free $pn \to np$ cross section $\left(\frac{d\sigma}{d\Omega}\right)^{\rm free}_{\rm pn}$ determined from Arndt phase shift [45] and values for $N_{\rm eff}$.

Although the four spectra were measured at very different energies the empirical values of k_F and $N_{\rm eff}$ are quite comparable. Especially, there is almost no variation for the value of $N_{\rm eff}$ which may suggest that the nuclear depth probed by the nucleon projectile into the ^{12}C target is quite energy independent.

TABLE III. Results obtained in the analysis of ^{12}C(p,n) quasifree scattering at $q \approx 2$ fm^{-1} at the indicated proton beam energies. See text for details.

E_p (MeV)	q (fm^{-1})	$\omega^{\rm QF}_{\rm peak}$ (MeV)	$\left(\frac{d^2\sigma}{d\Omega dE}\right)^{\rm QF}_{\rm peak}$ $\left(\frac{\rm mb}{\rm sr\cdot MeV}\right)$	$\left(\frac{d\sigma}{d\Omega}\right)^{\rm QF}_{\rm intg}$ $\left(\frac{\rm mb}{\rm sr}\right)$	$\left(\frac{d\sigma}{d\Omega}\right)^{\rm free}_{\rm pn}$ [a] $\left(\frac{\rm mb}{\rm sr}\right)$	$N_{\rm eff}$
186	2.00	94.0	0.23	27.0	5.99	2.3
256	1.89	99.8	0.25	33.9	8.47	2.0
495	1.89	98.4	0.31	43.8	9.43	2.3
795	1.92	97.8	0.25	39.9	8.49	2.3

[a] Free $p(n,p)$ cross section values at the same q obtained from Arndt phase shift 1992.

VI. CONCLUSION

The QF data have been compared with calculations of different models. The effect of Pauli blocking on the integrated QF angular distribution is in excellent agreement with the simple Fermi gas model prediction, in nuclei such as ^{12,13}C and ^{10,11}B. This enhances our confidence that the QF fitting process employed in the present study has extracted the QF strength properly. However, we notice that for the lighter nuclei ^{6,7}Li, the statistics of the simple Fermi gas model breaks down in describing the shape of the integrated QF angular distribution. The polarization observables, in particular D_{NN} when compared with RPWIA calculations, indicate a definite preference of the pseudovector coupling over the pseudoscalar coupling, and that the reduced mass effect is more obviously seen in D_{NN} data than in A_Y data for $(\vec{p},\vec{n})$ reactions. The slab model provides QF spectra with shapes in good agreement with the data, while the overall magnitudes of the spectra are not correctly predicted and need a q-dependent normalization. Finally, one of the main features observed in the present QF scattering is that the difference in energy loss between the centroid of the QF peak position and the corresponding $q^2/2M$ value decreases with increasing values of momentum transfer. We plan to measure at $E_p = 200$ MeV the spin-longitudinal and spin-transverse response functions at a few momentum transfers, to have a better understanding of this effect, which is not seen in $(\vec{p},\vec{n})$ reactions at higher energies.

This work was supported in part by the NSF.

[1] H. Esbensen and G.F. Bertsch, Phys. Rev. C **34**, 1419 (1986).
[2] J.S. O'Connell *et al.*, Phys. Rev. C **35**, 1063 (1987); Phys. Rev. Lett. **53**, 1627 (1984).
[3] F.A. Brieva and A. Dellafiore, Nucl. Phys. **A292**, 445 (1977).
[4] E.J. Moniz *et al.*, Phys. Rev. Lett. **26**, 445 (1971).
[5] J.S. O'Connell and B. Schroeder, Phys. Rev. C **38**, 2447 (1988).
[6] C.J. Horowitz and D.P. Murdock, Phys. Rev. C **37**, 2032

(1988).
[7] G.C. Hillhouse and P.R. De Kock, Phys. Rev. C **49**, 391 (1994).
[8] W.M. Alberico, M. Ericson, and A. Molinari, Nucl. Phys. **A379**, 429 (1982).
[9] Z.E. Meziani *et al.*, Phys. Rev. Lett. **54**, 1233 (1985).
[10] I. Berqvist *et al.*, Nucl. Phys. **A469**, 648 (1987).
[11] T. Sams, in *Spin and Isospin in Nuclear Interactions*, edited by S.W. Wissink, C.D. Goodman, and G.E. Walker (Plenum Press, New York, 1991).
[12] C. Gaarde, Nucl. Phys. **A507**, 79c (1990).
[13] D. Prout *et al.* (unpublished).
[14] J. Wambach, Phys. Rev. C **46**, 807 (1992).
[15] T. Carey *et al.*, Phys. Rev. Lett. **53**, 144 (1984).
[16] L.B. Rees *et al.*, Phys. Rev. C **34**, 627 (1987).
[17] X.Y. Chen *et al.*, Phys. Rev. C **47**, 2159 (1993).
[18] C.J. Horowitz and J. Piekarewicz, Phys. Lett. B **301**, 321 (1993).
[19] G.E. Brown and J. Wambach, Nucl. Phys. **A568**, 895 (1994).
[20] M. Ichimura, in Proceedings of the Sixth Franco-Japanese Colloquium, Saint Malo, 1992, edited by N. Alamanos *et al.* (unpublished), p. 49.
[21] A. De Pace and M. Viviani, Phys. Rev. C **48**, 2931 (1993).
[22] V.R. Pandharipande *et al.*, Phys. Rev. C **49**, 789 (1994).
[23] M. Ericson, Phys. Rev. C **49**, R2293 (1994).
[24] L. Wang *et al.*, Phys. Rev. C **47**, 2123 (1993).
[25] L. Wang, Ph.D. thesis, Ohio University, 1993 (unpublished).
[26] T.N. Taddeucci *et al.*, Nucl. Instrum. Methods Phys. Res. Sect. A **241**, 448 (1985).
[27] A. Erell *et al.*, Phys. Rev. C **34**, 1822 (1986).
[28] K.J. Raywood *et al.*, Phys. Rev. C **41**, 2836 (1990).
[29] A.L. Fetter and J.D. Walecka, *Quantum Theory of Many Particle Systems* (McGraw-Hill, New York, 1971).
[30] C.J. Horowitz and M.J. Iqbal, Phys. Rev. C **33**, 2059 (1986).
[31] C.J. Horowitz and D.P. Murdock, Phys. Rev. C **37**, 2032 (1988).
[32] F.A. Brieva and W.G. Love, Phys. Rev. C **42**, 2573 (1990).
[33] G.F. Bertsch and O. Scholten, Phys. Rev. C **25**, 804 (1982).
[34] H. Esbensen and G.F. Bertsch, Ann. Phys. (N.Y.) **157**, 255 (1984).
[35] M. Ichimura *et al.*, in *Spin Observables of Nuclear Probes*, edited by C.J. Horowitz, C.D. Goodman, and George E. Walker (Plenum Press, New York, 1988), pp. 207–220; Phys. Rev. C **39**, 1446 (1989); M. Ichimura and K. Kawahigashi, *ibid.* **45**, 1822 (1992).
[36] R.J. Glauber and G. Matthiae, Nucl. Phys. **B21**, 135 (1970).
[37] P. Ring and P. Shuck, *The Nuclear Many Body Problem* (Springer-Verlag, New York, 1980).
[38] C.W. de Jager *et al.*, At. Data Nucl. Data Tables **14**, 479 (1974).
[39] H. Sakai, in Proceedings of the Symposium on Spin-Isospin Responses, Osaka, Japan, 1994 (unpublished); H. Otsu *et al.*, RCNP Annual Report 1992, Osaka, Japan.
[40] R.D. Smith, in *Spin Observables of Nuclear Probes* [35], p. 15.
[41] H. Esbensen, H. Toki, and G.F. Bertsch, Phys. Rev. C **31**, 1816 (1985).
[42] L. Bland (private communication).
[43] N.S. Chant and P.G. Roos, Phys. Rev. C **27**, 1060 (1983).
[44] M.M. Meier *et al.*, Nucl. Sci. Eng. **102**, 310 (1989).
[45] R.A. Arndt and L.D. Soper, *Scattering Analysis Interactive Dial-In program* (SAID) (SP92), Virginia Polytechnic Institute and State University (unpublished).